This article has been accepted for publication in a future issue of this journal, but has not been fully edited. Content may change prior to final publication. Citation information: DOI 10.1109/TSTE.2022.3175430, IEEE Transactions on Sustainable Energy

Continuous Hydrothermal Flexibility Coordination Under Wind Power Uncertainty

Christian Øyn Naversen, *Member, IEEE,* Masood Parvania, *Senior Member, IEEE,* Arild Helseth, *Senior Member, IEEE,* Hossein Farahmand, *Senior Member, IEEE*

***Abstract*—This paper proposes a stochastic continuous-time optimization model for coordinating the operation of flexibility reserve in a hybrid hydro-thermal-wind power system. The proposed continuous-time model captures the sub-hourly uncertainty and variations of wind power and load, and accurately models and schedules the ramping flexibility of the hydrothermal system to match the uncertainty and variations of wind power and load. A simplified Northern European system is studied over a 30-hour period to examine the potential of using hydropower as a comprehensive flexibility provider. Norwegian hydropower is shown to be a significant source of flexibility used to mitigate wind power variations, especially during ramping constrained periods. The hydropower provides 73.5% of the balancing energy in the base case, which includes smoothing out longer wind power deviations as well as rapid ramping relief. The short-term implications of increasing the offshore wind power in the North Sea by 50% compared to 2020 was also studied in the Northern European test system. The increased wind power causes steeper ramping in the net load, which drives the hydropower to its full balancing potential to allow thermal units to operate within their ramping limits.**

***Index Terms*—Hydrothermal scheduling, hydropower, wind power, flexibility reserve, continuous-time scheduling.**

NOMENCLATURE

Sets and Indices

$\mathcal{J}$	Thermal generators, index j
$\mathcal{K}$	Water value cuts, index k
$\mathcal{L}$	HVDC cables, index l
$\mathcal{M}$	Hydropower plant-reservoir pairs, index m
$\mathcal{A}$	Areas in the system, index a
$\mathcal{I}_m^{d/b/o}$	Reservoirs that discharge/bypass/spill into m, index i
$\mathcal{S}$	Second-stage scenarios, index s
$\mathcal{T}$	Time intervals, index h

Main Variables

f_{lh}	Flow on HVDC cable	[MW]
g_{jh}	Generated thermal power	[MW]
p_{mh}	Generated hydropower	[MW]
q^{in}_{mh}	Total controlled flow into reservoir	[m^3/s]
q^{net}_{mh}	Net flow into reservoir	[m^3/s]
q^{rel}_{mh}	Total flow released out of reservoir	[m^3/s]
q^{b}_{mh}	Flow through bypass gate	[m^3/s]
q^{d}_{mh}	Flow through turbine	[m^3/s]
q^{o}_{mh}	Flow through spill gate	[m^3/s]
$r^{\text{hyd},\uparrow/\downarrow}_{mh}$	Reserved hydropower capacity up/down	[MW]
$r^{\text{th},\uparrow/\downarrow}_{jh}$	Reserved thermal capacity up/down	[MW]
$su^{\text{th}}_{jh}, sd^{\text{th}}_{jh}$	Startup, shutdown of thermal generator	[MW]
$su^{\text{hyd}}_{mh}, sd^{\text{hyd}}_{mh}$	Startup, shutdown of hydropower plant	[MW]
u^{hyd}_{mh}	Hydropower unit commitment decision	
u^{th}_{jh}	Thermal unit commitment decision	
v_{mh}	Reservoir volume at time interval start	[m^3]
w_{mh}	Reservoir volume within time interval	[m^3]
y^{crt}_{sah}	Power curtailment	[MW]
y^{shd}_{sah}	Load shedding	[MW]
z_s	Future expected system cost	[€]

Main Parameters

ΔW_{sah}	Wind power scenario deviation	[MW]
δ_h	Length of time interval	[s]
η_m	Hydropower efficiency	[MWs/m^3]
$\gamma^{\uparrow/\downarrow}_{jh}$	Thermal ramping increase for start/stop	[MW/s]
$\overline{C}^{\text{th}}_j, \underline{C}^{\text{th}}_j$	Thermal startup, shutdown cost	[€]
$\overline{C}^{\text{hyd}}_m, \underline{C}^{\text{hyd}}_m$	Hydro startup, shutdown cost	[€]
π_s	Scenario probability	
C^{crt}	Power curtailment cost	[€/m^3]
C^{shd}	Load shedding cost	[€/m^3]
C^b	Penalty for bypassing water	[€/MW]
C^o	Penalty for spilling water	[€/MW]
C_j	Marginal cost of thermal generator	[€/MW]
D_k	Water value cut constant	[€]
F^{max}_l	Maximal flow limit on HVDC cable	[MW]
$G^{max/min}_j$	Maximal/minimal thermal capacity	[MW]
G_{la}	Grid coefficient determining cable flow direction	
I^u_{mh}	Natural inflow from creek intakes	[m^3/s]
I_{mh}	Natural inflow into reservoir	[m^3/s]
K^{th}_j	Thermal reserve capacity cost	[€/MW]
K^{hyd}_m	Hydro reserve capacity cost	[€/MW]
L_{ah}	Forecasted load	[MW]
N	Number of time intervals in $\mathcal{T}$	
$P^{max/min}_m$	Maximal/minimal hydropower capacity	[MW]
Q^b_m	Maximal flow through bypass gate	[m^3/s]
Q^d_m	Maximal flow through turbine	[m^3/s]
$R^{\uparrow/\downarrow}_j$	Thermal unit ramping limits	[MW/s]
V^0_m	Initial reservoir volume	[m^3]
V_m	Maximal reservoir capacity	[m^3]

This work was funded by The Research Council of Norway, Project No.268014/E20.

C. Ø. Naversen is with the Department of Electric Power Engineering, Norwegian University of Science and Technology, Trondheim, Norway, and also the Department of Energy Systems, SINTEF Energy Research, Trondheim, Norway (e-mail: christian.naversen@sintef.no).

H. Farahmand is with the Department of Electric Power Engineering, Norwegian University of Science and Technology, Trondheim, Norway (e-mail: hossein.farahmand@ntnu.no).

A. Helseth is with the Department of Energy Systems, SINTEF Energy Research, Trondheim, Norway (e-mail: Arild.Helseth@sintef.no).

M. Parvania is with the Department of Electrical and Computer Engineering, The University of Utah, Salt Lake City, UT 84112 USA (email: masood.parvania@utah.edu).

W_{ah}	Forecasted wind power	[MW]
WV_{mk}	Water value cut coefficient	[€/m^3]

I. Introduction

A. Motivation

THE transition from traditional power systems dominated by conventional power generation to hybrid energy systems with significant amounts of variable renewable energy sources (VRES) is well underway in many power systems around the world. Such a fundamental shift is an important part of eventually reaching a net-zero emission and climate-neutral society, which is currently the stated long-term goal of the European Union [1].

There are several new challenges related to operating a hybrid power system, mainly related to the variability of renewable resources. Optimal coordination between different resources to mitigate the low flexibility of VRES is a central issue. The problem requires detailed modelling of the responsiveness of each generation technology in the system to fairly estimate their combined flexibility, or lack thereof. The stochastic nature of VRES must also be considered in the scheduling of power production and reserve capacity, as forecast errors will inevitably cause deviations between scheduled production and actual net load. Such imbalances can be modelled through stochastic optimization techniques, and are an essential driver behind the advancement of stochastic scheduling models in the last decades [2].

In addition to limited resource flexibility, hybrid systems are faced with the challenge of adapting to the current electricity market structure to handle ramping scarcity in real-time balancing. The day-ahead electricity markets in Europe typically have a time resolution of 15, 30, or 60 minutes, which results in piece-wise constant production schedules for each time interval after the market is cleared [3]. Even if the load and VRES power production were perfectly deterministic, the discrete market structure creates a type of structural power imbalances because the net load is a continuous function of time. Structural imbalances exhibit a largely deterministic behavior as they are occur in the transition from one market bid interval to the next [4], [5]. Regulatory changes such as finer market trading granularity could alleviate some structural imbalances [6], though moving from trading energy to power profiles should be considered [7].

An example of a large hybrid system is the interconnected power system in Northern Europe, which contains flexible hydropower in Norway with large and cascaded reservoirs, and conventional thermal generation in Continental Europe with considerable emerging offshore wind power resources in the North Sea [8]. The growth in high-voltage direct current (HVDC) transmission capacity from Norway to continental Europe and Great Britain increases the potential for utilizing the hydropower flexibility to help balance the larger system. The role of hydropower as a large-scale flexibility provider will become more valuable as the transition towards a carbon-neutral power system continues. To harness and transport the hydropower flexibility across country lines, it is critical to develop modelling tools that can take a holistic approach to short-term balancing of both structural imbalances and stochastic VRES forecast deviations.

B. Literature Survey

The operational planning of hydrothermal systems has been investigated over several decades, resulting in various well-established models. Long-term scheduling models such as [9] and [10] focus on calculating prices and finding the optimal long-term reservoir strategy given the seasonal weather uncertainties. Medium-term models such as [11] refine the long-term strategy and pass it to the short-term operational models like [12], which translate it into market bids and production plans for tomorrow. However, these traditional hydrothermal optimization models are based on discretizing the optimization horizon into time intervals with piece-wise constant power generation. Such models are unable to properly capture the rapid changes in VRES power production and the ramping limitations of the power generation in the system.

The problem of the hidden inflexibility in traditional optimization models has led to research on power-based unit commitment (UC) models where the power generation is no longer assumed to be constant through the time interval. Allowing linear power production profiles is the simplest extension of the energy-based UC formulation and was shown to perform better than both deterministic and stochastic energy-based UC models in [13]. Continuous-time optimization was first introduced to power system operation in [14], [15], and generalizes the idea of power-based optimization models. Bernstein polynomials are used to describe the time-dependent decision variables in the models, while it is still possible to solve them as mixed-integer linear programs (MILPs), unlike related non-linear model formulations in adjacent fields such as [16]. The framework enables the modelling of flexible and inflexible units in a more realistic way than standard discrete-time models and can capture high-ramping events in VRES production.

Stochastic continuous-time models have been formulated previously to account for the uncertainty of VRES power generation. The multi-stage stochastic model in [17], [18] are examples of this. The stochastic model in [18] uses different fidelity for the polynomial expansion in the first and second stage problem formulations to allow higher variations in the realized net load. A flexibility reserve product that provides reserve capacity for both energy and ramping relief is formulated in the stochastic continuous-time model found in [19], which also incorporates energy storage. Hydropower in cascaded topology, however, is fundamentally different from a energy storage system due to the physical dynamics between different reservoirs and hydropower's large energy storage potential. The cascaded hydropower generation is modeled in a deterministic continuous-time framework in [20]. The case study in [21] shows that the deterministic hydrothermal continuous-time model was able to coordinate flexibility and avoid abrupt flow changes on HVDC lines due to rapid fluctuations in wind power compared to a discrete-time UC model of 15-min resolution. Although generic energy storage systems are modeled in the stochastic optimization frameworks

in [17], [18], no previous work has attempted to include large-scale hydropower in a cascaded topology into a stochastic continuous-time model, which is pursued in this paper.

C. Contributions

This paper develops a stochastic continuous-time model for coordinating the operation of cascaded hydropower units with considerable storage capacity, thermal generation with limited flexibility, and uncertain wind power. The proposed model represents a fundamental approach to the problem of coordinating flexibility in a hybrid power system over very short and intermediate time scales. The flexible hydropower can be used both for ramping flexibility within a time interval (hour) and for shifting production to accommodate forecast errors in wind power. Compared to the deterministic models published in the authors' previous work in [20], [21], several new modifications to the continuity constraints are required to achieve a tractable and flexible hydropower formulation when uncertainty is added. This includes formulating the continuity constraints over the branching point of the scenario tree through simple initial conditions on the second-stage variables. The results from the case study show how the model uses the hydropower resources for both ramping relief and large-scale wind energy balancing, contributing up to 73.5% of the total balancing energy of the system. When the installed wind power capacity is increased by 50%, the hydropower is pushed towards its limits for providing balancing services, constrained by both HVDC transmission capacity and internal power limits. The proposed model can thus be used to gain insight into the short-term flexibility limits and capabilities of hybrid power systems, which will be highly relevant for both system operators and power producers.

In summary, the main contributions of this paper include:

- The paper presents a new stochastic continuous-time optimization framework, which includes a detailed hydropower description in a cascaded topology.
- The proposed framework represents a holistic approach to short-term hybrid power system balancing with hydropower. Both structural market imbalances and stochastic imbalanced caused by VRES forecast errors are dealt with by the modeling.
- The proposed model provides new insights to understand the short-term impacts of incorporating high amounts of offshore wind in an interconnected hybrid power system with significant hydropower resources.

D. Organization of the Paper

The rest of this paper is organized as follows: The proposed stochastic continuous-time model is formulated in Section II and the cases study based on the Northern European power system is presented in Section III. Concluding remarks and ideas for future work are found in Section IV, and the fundamental properties of continuous-time optimization models are described in Appendix A.

II. The Proposed Optimization Model

A two-stage continuous-time unit commitment and reserve procurement model for a hydrothermal system with offshore wind power joined by HVDC cables is formulated in Sections II-A to II-C. The main assumption of the proposed model is that the operation of the hybrid power system can be modelled by minimizing the total operational system costs of thermal and hydropower units, while aiming to procure flexibility for minimizing the wind curtailment in the system. The load in each area is assumed to be deterministic, and only the uncertainty in wind power generation is considered in the formulation. The continuous-time formulation of the model also assumes that all temporal data can be represented as continuous and smooth functions in time of a finite degree [18]. However, the assumption of continuity is relaxed for the optimal hydropower production schedule and related quantities as detailed further in Section II.

The mathematical formulation of the proposed model represents the short-term operation of the hybrid system considering system dispatch under wind power uncertainty, followed by real-time balancing. The overall goal of the model is to minimize the cost of unit commitment, energy production, and reserve procurement for the whole system given uncertainty in the wind power production. The most important first-stage decisions are thus to determine the unit commitment, production schedules, and reserve capacity allocation of all units, in addition to the scheduled flow on the cables between the areas. The uncertainty in wind power generation is realized in the second stage, and so the procured reserve capacity from the first stage is activated to balance the deviation. Respecting the physical constraints of the system and individual units, such as ramping on thermal units and the water balance of the hydropower system, is essential in both the scheduling and balancing stages. Wind power is considered to be known for a short period at the beginning of the optimization horizon before branching into several possible scenarios, giving rise to the two-stage formulation.

The variables of the model are written as lower case Latin letters, and variables and other symbols in bold signify a column vector representing the coefficients of the underlying Bernstein polynomials. This matrix notation is used throughout the paper and is explained in detail in Appendix A. The model formulation is organized into three main parts: Section II-A describes the objective function, while Section II-B and Section II-C describe the first-stage and second-stage constraints of the model, respectively. Section II-B and Section II-C are further split into subsections that formulate the constraints related to thermal units, the hydropower topology, and system wide constraints. In addition, Section II-C4 defines the continuity constraints necessary to enforce a smooth transition from the initial deterministic time period to the time period with uncertain wind power production.

A. Objective Function

The objective function Ω for the stochastic model is to minimize the total expected cost of operating the interconnected

This article has been accepted for publication in a future issue of this journal, but has not been fully edited. Content may change prior to final publication. Citation information: DOI 10.1109/TSTE.2022.3175430, IEEE Transactions on Sustainable Energy

hydrothermal system:

$$\begin{aligned}\min \Omega = \frac{1}{4}\mathbf{1}^\intercal \sum_{h\in\mathcal{T}} \delta_h \Bigg[\sum_{m\in\mathcal{M}} \left(C^b \mathbf{q}^b_{mh} + C^o \mathbf{q}^o_{mh} \right) + \sum_{j\in\mathcal{J}} C_j \mathbf{g}_{jh} \\ + \sum_{m\in\mathcal{M}} K^{\text{hyd}}_m \left(\mathbf{r}^{\text{hyd},\uparrow}_{mh} + \mathbf{r}^{\text{hyd},\downarrow}_{mh} \right) + \sum_{j\in\mathcal{J}} K^{\text{th}}_j \left(\mathbf{r}^{\text{th},\uparrow}_{jh} + \mathbf{r}^{\text{th},\downarrow}_{jh} \right) \Bigg] \\ + \sum_{h\in\mathcal{T}} \sum_{m\in\mathcal{M}} \left(\overline{C}^{\text{hyd}}_m su^{\text{hyd}}_{mh} + \underline{C}^{\text{hyd}}_m sd^{\text{hyd}}_{mh} \right) \\ + \sum_{h\in\mathcal{T}} \sum_{j\in\mathcal{J}} \left(\overline{C}^{\text{th}}_j su^{\text{th}}_{jh} + \underline{C}^{\text{th}}_j sd^{\text{th}}_{jh} \right) + \sum_{s\in\mathcal{S}} \pi_s \Delta\Omega_s. \end{aligned} \tag{1}$$

The first-stage variables are expressed with Bernstein polynomials of degree three, while the second-stage variables are of fidelity five. The higher fidelity in the second stage makes it possible to model higher levels of variability in the wind power. The first line of the objective is the total incurred spillage and bypass penalties, and the scheduled cost of the thermal generation. Bypass and spillage penalties are incurred when water is bypassed around the power plant or spilled out of the reservoir, respectively. Figure 1 illustrates how the different waterways are modelled. As in [18], an explicit cost for the reserved hydropower capacity and thermal capacity is added in the second line of the objective function. The cost is assumed to be constant over the optimization horizon and equal for upward and downward reserves. The total objective function cost has been calculated by integrating the time-varying and continuous curves of third degree over the whole optimization horizon by use of (16) in Appendix A. The startup and shutdown costs of the thermal and hydropower plants are summed up in the third and fourth lines, while the last term in the fourth line of (1) is the expected cost of the balancing stage. The cost $\Delta\Omega_s$ is the second-stage objective function cost in scenario $s \in \mathcal{S}$ with probability π_s, which is the sum of penalties and operational cost of the thermal and hydropower plants:

$$\begin{aligned}\Delta\Omega_s = z_s + \frac{1}{6}\mathbf{1}^\intercal \sum_{h\in\mathcal{T}} \delta_h \Bigg[\rho^{\text{hyd}} \sum_{m\in\mathcal{M}} \left(\Delta\mathbf{p}^+_{smh} + \Delta\mathbf{p}^-_{smh} \right) \\ + \sum_{j\in\mathcal{J}} \left(C^+_j \Delta\mathbf{g}^+_{sjh} - C^-_j \Delta\mathbf{g}^-_{sjh} \right) \\ + \sum_{m\in\mathcal{M}} \left(C^{o+} \Delta\mathbf{q}^{o+}_{smh} - C^{o-} \Delta\mathbf{q}^{o-}_{smh} \right) \\ + \sum_{m\in\mathcal{M}} \left(C^{b+} \Delta\mathbf{q}^{b+}_{smh} - C^{b-} \Delta\mathbf{q}^{b-}_{smh} \right) \\ + \sum_{a\in\mathcal{A}} \left(C^{\text{shd}} \mathbf{y}^{\text{shd}}_{sah} + C^{\text{crt}} \mathbf{y}^{\text{crt}}_{sah} \right) \Bigg]. \end{aligned} \tag{2}$$

The expected future cost of the system and the deployment cost of the activated hydropower reserves ($\Delta\mathbf{p}^{\pm}_{smh}$) make up the terms in the first line of (2). The expected future system cost z_s is bounded by linear constraints calculated by long-term hydrothermal models such as [9], which are described further in Section II-C3. Note that some of the second-stage variables are formulated as deviations from the first-stage variables with a preceding Δ symbol, and are therefore not listed in the nomenclature. The cost of activating hydropower reserves ρ^{hyd} is the same in both directions and considered equal for all hydropower units. The operational and deployment cost of the thermal reserves ($\Delta\mathbf{g}^{\pm}$) is found in the second line, where the cost coefficients $C^{\pm}_j$ are related to the marginal cost C_j of the thermal units so that $C^-_j < C_j < C^+_j$. This means that a deployment cost is paid when reserves are deployed in either direction in addition to the change in operational cost of the thermal units compared to the scheduled production cost[1]. Line three and four of the second-stage objective function apply the same cost structure to changing the bypass ($\Delta\mathbf{q}^{b\pm}_{smh}$) and spillage ($\Delta\mathbf{q}^{o\pm}_{smh}$) flows in the second stage. This is done to discourage the model from unnecessary changes in the bypass and spillage decisions in the balancing stage. Finally, the last line of (2) is the cost of shedding load and curtailing wind in all areas.

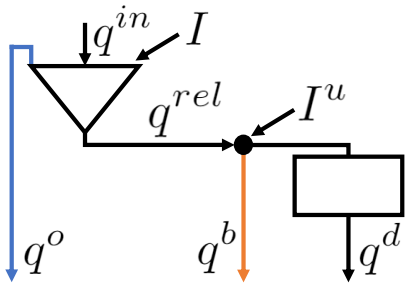

Fig. 1. Depiction of the different waterways for discharging, bypassing and spilling water between reservoirs. Natural inflow enters the system in two different ways, either into the reservoir (triangle) or directly into the main tunnel of the plant (rectangle).

B. First-Stage Constraints

The first-stage constraints model the unit commitment decisions, reserve procurement, and production scheduling decisions of the interconnected system. A continuous-time formulation of third degree is used to model the first-stage constraints.

1) Thermal production constraints: All thermal generators are scheduled according to the following unit commitment and ramping constraints:

$$\mathbf{g}_{jh} + \mathbf{r}^{\text{th},\uparrow}_{jh} \leq G^{max}_j \mathbf{u}^{\text{th}}_{jh} \tag{3a}$$
$$\mathbf{g}_{jh} - \mathbf{r}^{\text{th},\downarrow}_{jh} \geq G^{min}_j \mathbf{u}^{\text{th}}_{jh} \tag{3b}$$
$$\mathbf{0} \leq \mathbf{r}^{\text{th},\uparrow/\downarrow}_{jh} \leq \left(G^{max}_j - G^{min}_j \right) \mathbf{1} \tag{3c}$$
$$\mathbf{u}^{\text{th}}_{jh} = \left[u^{\text{th}}_{jh}, u^{\text{th}}_{jh}, u^{\text{th}}_{j,h+1}, u^{\text{th}}_{j,h+1} \right]^\intercal \tag{3d}$$
$$\mathrm{F}^0(\mathbf{g}_{jh}) = 0, \quad h \neq N \tag{3e}$$
$$\mathrm{F}^1(\mathbf{g}_{jh}) = 0, \quad h \neq N \tag{3f}$$
$$su^{\text{th}}_{jh} - sd^{\text{th}}_{jh} = u^{\text{th}}_{j,h+1} - u^{\text{th}}_{jh} \tag{3g}$$
$$-\mathbf{R}^{\downarrow}_{jh} \leq \frac{1}{\delta_h} \mathbf{K}^\intercal_3 \cdot \mathbf{g}_{jh} \leq \mathbf{R}^{\uparrow}_{jh} \tag{3h}$$

[1]Note that the negative sign for $C^-_j \Delta g^-_{sjh}$ in (2) means that some of the scheduled thermal fuel costs are recovered when regulating down, but a premium balancing cost is still payed since $C^-_j < C_j$.

$$\mathbf{R}^{\uparrow}_{jh} = R^{\uparrow}_{j}\left[u^{\text{th}}_{jh}, u^{\text{th}}_{j,h+1} + \gamma^{\uparrow}_{jh} su^{\text{th}}_{jh}, u^{\text{th}}_{j,h+1}\right]^{\intercal} \tag{3i}$$

$$\mathbf{R}^{\downarrow}_{jh} = R^{\downarrow}_{j}\left[u^{\text{th}}_{jh}, u^{\text{th}}_{jh} + \gamma^{\downarrow}_{jh} sd^{\text{th}}_{jh}, u^{\text{th}}_{j,h+1}\right]^{\intercal} \tag{3j}$$

$$u^{\text{th}}_{jh} \in \{0,1\} \tag{3k}$$

$$0 \leq su^{\text{th}}_{jh}, sd^{\text{th}}_{jh} \leq 1 \tag{3l}$$

$$\{su^{\text{th}}_{jh}, sd^{\text{th}}_{jh}\} \text{ of SOS type 1.} \tag{3m}$$

Theses constraints are primarily based on the formulation of [15]. The thermal generation and the procured reserve capacity in the upward and downward direction must obey the minimum and maximum generation limits of the generator in (3a)–(3c). Note that the convex hull property in (13) in Appendix A is used to ensure that the continuous curves represented by the coefficient vectors are within the generator bounds. The binary commitment variable u^{th}_{jh} can be interpreted as the commitment status of the generator at the beginning of interval h, and is incorporated into the generation limit constraints by the vector in (3d). Note that this formulation requires $N+1$ commitment variables for each generator, as the commitment status at the end of the horizon is included. The formulation allows the thermal units to use the whole interval h to smoothly start up or shut down production, which is necessary since the generation trajectory is required to be C^1 continuous by (3e)–(3f). The startups and shutdowns of the generators are counted in (3g). The ramping constraints for the generators are formulated in (3h), which is based on taking the derivative of the thermal production trajectory $g_j(t)$ and using the relation in (14) in Appendix A. The upper and lower ramping trajectory bounds are formulated in (3i) and (3j). The commitment variables are used to make a tight formulation of the ramping constraint. Extra care must be taken for the middle vector component to ensure that the ramping constraints do not interfere with the upper and lower generation bounds when a unit starts up or shuts down. Additional ramping capability $\gamma^{\uparrow/\downarrow}_{jh} R^{\uparrow/\downarrow}_{j}$ is used to relax the ramping constraint in this case, and must satisfy $\gamma^{\uparrow/\downarrow}_{jh} \geq \frac{3G^{min}_{j}}{\delta_h R^{\uparrow/\downarrow}_{j}} - 1$ for the unit to be able to start up or shut down. The startup and shutdown variables are formulated as continuous variables which are part of a special ordered set (SOS) of type 1 in (3l)–(3m), which means that at most one of the variables for each $j \in \mathcal{J}$ and $h \in \mathcal{T}$ can be nonzero.

2) Hydropower constraints: The constraints governing the management of the hydropower plants and reservoirs are given in (4a)–(4t) and based on the formulation in [20]:

$$v_{m0} = V^0_m \tag{4a}$$

$$v_{m,h+1} - v_{mh} = \frac{1}{4}\delta_h \mathbf{1}^{\intercal} \cdot \mathbf{q}^{\text{net}}_{mh} \tag{4b}$$

$$\mathbf{w}_{mh} = v_{mh}\mathbf{1} + \delta_h \mathbf{N}^{\intercal}_{3} \cdot \mathbf{q}^{\text{net}}_{mh} \tag{4c}$$

$$\mathbf{q}^{\text{net}}_{mh} = \mathbf{I}_{mh} + \mathbf{q}^{\text{in}}_{mh} - \mathbf{q}^{\text{rel}}_{mh} - \mathbf{q}^{o}_{mh} \tag{4d}$$

$$\mathbf{q}^{\text{in}}_{mh} = \sum_{i \in \mathcal{I}^d_m} \mathbf{q}^{d}_{ih} + \sum_{i \in \mathcal{I}^b_m} \mathbf{q}^{b}_{ih} + \sum_{i \in \mathcal{I}^o_m} \mathbf{q}^{o}_{ih} \tag{4e}$$

$$\mathbf{q}^{\text{rel}}_{mh} = \mathbf{q}^{d}_{mh} + \mathbf{q}^{b}_{mh} - \mathbf{I}^{u}_{mh} \tag{4f}$$

$$\mathbf{p}_{mh} = \eta_m \mathbf{q}^{d}_{mh} \tag{4g}$$

$$\mathbf{p}_{mh} + \mathbf{r}^{\text{hyd},\uparrow}_{mh} \leq P^{max}_{m} u^{\text{hyd}}_{mh}\mathbf{1} \tag{4h}$$

$$\mathbf{p}_{mh} - \mathbf{r}^{\text{hyd},\downarrow}_{mh} \geq P^{min}_{m} u^{\text{hyd}}_{mh}\mathbf{1} \tag{4i}$$

$$su^{\text{hyd}}_{mh} - sd^{\text{hyd}}_{mh} = u^{\text{hyd}}_{m,h+1} - u^{\text{hyd}}_{mh}, \;\; h \neq N \tag{4j}$$

$$\text{F}^0(\mathbf{q}^{o}_{mh}) = 0, \;\; h \neq N \tag{4k}$$

$$\text{F}^0(\mathbf{q}^{b}_{mh}) = 0, \;\; h \neq N \tag{4l}$$

$$\mathbf{0} \leq \mathbf{w}_{mh} \leq V_m\mathbf{1} \tag{4m}$$

$$\mathbf{0} \leq \mathbf{q}^{d}_{mh} \leq Q^{d}_{m}\mathbf{1} \tag{4n}$$

$$\mathbf{0} \leq \mathbf{q}^{b}_{mh} \leq Q^{b}_{m}\mathbf{1} \tag{4o}$$

$$\mathbf{0} \leq \mathbf{q}^{o}_{mh}, \mathbf{q}^{\text{rel}}_{mh} \tag{4p}$$

$$\mathbf{0} \leq \mathbf{r}^{\text{hyd},\uparrow/\downarrow}_{mh} \leq \left(P^{max}_{m} - P^{min}_{m}\right)\mathbf{1} \tag{4q}$$

$$u^{\text{hyd}}_{mh} \in \{0,1\} \tag{4r}$$

$$0 \leq su^{\text{hyd}}_{mh}, sd^{\text{hyd}}_{mh} \leq 1 \tag{4s}$$

$$\{su^{\text{hyd}}_{mh}, sd^{\text{hyd}}_{mh}\} \text{ of SOS type 1.} \tag{4t}$$

The volume balance of the reservoirs is kept by (4a) and (4b), where the volume variables v_{mh} is the volume at the start of interval h. The change in volume over a time interval is found by integrating the net flow into the reservoir by using the relation in (16) in Appendix A. The time-varying volume within time interval h is found by using (15) in Appendix A, and is described by $\mathbf{w}_{mh}$ in (4c). Equations (4d)–(4f) describe how water can flow through the three different waterways between reservoirs, see Figure 1 for an illustration. All waterways may lead to different downstream reservoirs or directly out of the system. The regulated flow into the reservoir is found by summing up the discharge, bypass and spillage flows from the connected upstream reservoirs. It is necessary to introduce the water released from the reservoir ($\mathbf{q}^{\text{rel}}_{mh}$) to properly model the unregulated inflow which enters the system between the reservoir and plant. Regulated inflow enters directly into the reservoirs and may therefore be stored. The power output of the generator is approximated as linearly related to the discharged water through the turbine in (4g). Due to the large problems size, the hydropower production function is assumed to be concave, see [22] for more accurate treatment. The unit commitment and startup/shutdown constraints are found in (4h)–(4j), which includes the spinning reserve capacity procurement and the binary commitment status. Note that the upper and lower generation limits of the hydropower units are not modelled in the same way as the thermal units in (3a) and (3b). Since starting a hydropower unit usually takes less than a minute, the hydropower production trajectories are not required to be continuous over time intervals. Consequently, the hydropower units are allowed to instantaneously start up or shut down production from one interval to the next. The bypass and spillage variables are still forced to be C^0 continuous in (4k) and (4l). The remaining constraints (4m)–(4t) are the imposed physical bounds for the variables.

3) System constraints: System wide constraints for the areas connected by HVDC transmission lines are the following:

$$\sum_{m \in \mathcal{M}_a} \mathbf{p}_{mh} + \sum_{j \in \mathcal{J}_a} \mathbf{g}_{jh} - \sum_{l \in \mathcal{L}} G_{la}\mathbf{f}_{lh} = \mathbf{L}_{ah} - \mathbf{W}_{ah} \tag{5a}$$

$$-F^{max}_{l}\mathbf{1} \leq \mathbf{f}_{lh} \leq F^{max}_{l}\mathbf{1} \tag{5b}$$

$$\text{F}^0(\mathbf{f}_{lh}) = 0, \;\; h \neq N \tag{5c}$$

$$\mathrm{F}^1(\mathbf{f}_{lh}) = 0, \;\; h \neq N \tag{5d}$$

$$\sum_{j \in \mathcal{J}} \mathrm{F}^0(\mathbf{r}_{jh}^{\mathrm{th},\uparrow/\downarrow}) = 0, \;\; h \neq N \tag{5e}$$

$$\sum_{m \in \mathcal{M}} \mathrm{F}^0(\mathbf{r}_{mh}^{\mathrm{hyd},\uparrow/\downarrow}) = 0, \;\; h \neq N. \tag{5f}$$

The load and forecasted wind power are C^1 continuous input parameters, and must be balanced by the total thermal and hydropower generation in each area in addition to the imports and exports on the transmission lines in (5a). The coefficient G_{la} is either ± 1 or 0, and dictates the positive flow direction on line l if it is connected to area a. Equation (5b) bounds the maximal and minimal flow on each transmission line, and (5c) and (5d) force the line flow to be C^1 continuous. Even though the individual hydropower production variables are discontinuous over time interval shifts, the C^1 continuity of all other components of the power balance constraint forces the sum of the hydropower production to be C^1 continuous. The total reserved thermal and hydropower capacity in both directions is required to be C^0 continuous in (5e) and (5f).

C. Second-Stage Constraints

The uncertain wind power generation is realized in the second stage, and the reserved capacity of the generators of the system is deployed to keep the system in balance. The first h_0 time intervals of the optimization horizon is considered deterministic with known wind power output, which makes it possible to model a smooth transition of the uncertain wind power from time h_0. The second-stage variables are therefore only defined for the time periods $h \in \{h_0, \ldots, N\} \equiv \mathcal{T}_{scen}$. The second-stage variables are formulated as deviations from their first-stage values where applicable, signified by a preceding Δ symbol. The connection to the first-stage production schedule, reserve capacity procurement, and unit commitment decisions make up the tightest coupling between the stages. However, the first-stage water flow and reservoir volume plans also affect the second-stage hydropower operation, as shown in Section II-C2. The constraints listed in the following subsections are valid for all scenarios $s \in \mathcal{S}$, and scenario dependent data and decision variables are marked by a scenario subscript s. The time-dependent scenario variables are modelled using 5th degree Bernstein polynomials to capture the fast variations of the wind power production.

1) Thermal production constraints: The constraints dictating the change in thermal production as reserve capacity is deployed are valid for all thermal generators and time intervals $h \in \mathcal{T}_{scen}$:

$$-\mathbf{X}_{3,5}^{\intercal} \cdot \mathbf{r}_{jh}^{\mathrm{th},\downarrow} \leq \Delta\mathbf{g}_{sjh} \leq \mathbf{X}_{3,5}^{\intercal} \cdot \mathbf{r}_{jh}^{\mathrm{th},\uparrow} \tag{6a}$$

$$\frac{1}{\delta_h}\mathbf{K}_5^{\intercal} \cdot \left(\mathbf{X}_{3,5}^{\intercal} \cdot \mathbf{g}_{jh} + \Delta\mathbf{g}_{sjh}\right) \leq \mathbf{X}_{2,4}^{\intercal} \cdot \mathbf{R}_{jh}^{\uparrow} \tag{6b}$$

$$\frac{1}{\delta_h}\mathbf{K}_5^{\intercal} \cdot \left(\mathbf{X}_{3,5}^{\intercal} \cdot \mathbf{g}_{jh} + \Delta\mathbf{g}_{sjh}\right) \geq -\mathbf{X}_{2,4}^{\intercal} \cdot \mathbf{R}_{jh}^{\downarrow} \tag{6c}$$

$$\mathrm{F}^0(\Delta\mathbf{g}_{sjh}) = 0, \;\; h \neq N \tag{6d}$$

$$\mathrm{F}^1(\Delta\mathbf{g}_{sjh}) = 0, \;\; h \neq N \tag{6e}$$

$$\Delta\mathbf{g}_{sjh} = \Delta\mathbf{g}_{sjh}^{+} - \Delta\mathbf{g}_{sjh}^{-} \tag{6f}$$

$$\mathbf{0} \leq \Delta\mathbf{g}_{sjh}^{\pm}. \tag{6g}$$

The deployed thermal reserve power $\Delta\mathbf{g}_{sjh}$ is bound to be within the limits determined by the first-stage reserve procurement in Section II-B1. The elevation matrix $\mathbf{X}_{3,5}$ is used to lift the first-stage reserve variables to the higher fidelity of the second-stage variables. Ramping constraints are applied to the entire second-stage generation in (6b) and (6c) that enforce the same upper and lower ramping trajectories as in the first-stage constraints (3i) and (3j). The second-stage change in production is required to be C^1 continuous in (6d) and (6e), and is explicitly split into positive and negative parts $\Delta\mathbf{g}_{sjh}^{\pm}$ in (6f) and (6g) to distinguish upward and downward reserve activation.

2) Hydropower constraints: The second-stage hydropower related decisions for all time intervals $h \in \mathcal{T}_{scen}$ are also formulated as deviations from the first-stage solution governed by the constraints in Section II-B2:

$$\Delta v_{sm,h_0} = 0 \tag{7a}$$

$$\Delta v_{sm,h+1} - \Delta v_{smh} = \frac{1}{6}\delta_h \mathbf{1}^{\intercal} \cdot \Delta\mathbf{q}_{smh}^{\mathrm{net}} \tag{7b}$$

$$\Delta\mathbf{w}_{smh} = \Delta v_{smh}\mathbf{1} + \delta_h \mathbf{N}_5^{\intercal} \cdot \Delta\mathbf{q}_{smh}^{\mathrm{net}} \tag{7c}$$

$$\Delta\mathbf{q}_{smh}^{\mathrm{net}} = \Delta\mathbf{q}_{smh}^{\mathrm{in}} - \Delta\mathbf{q}_{smh}^{\mathrm{rel}} - \Delta\mathbf{q}_{smh}^{o} \tag{7d}$$

$$\Delta\mathbf{q}_{smh}^{\mathrm{in}} = \sum_{i \in \mathcal{I}_m^d} \Delta\mathbf{q}_{sih}^{d} + \sum_{i \in \mathcal{I}_m^b} \Delta\mathbf{q}_{sih}^{b} + \sum_{i \in \mathcal{I}_m^o} \Delta\mathbf{q}_{sih}^{o} \tag{7e}$$

$$\Delta\mathbf{q}_{smh}^{\mathrm{rel}} = \Delta\mathbf{q}_{smh}^{d} + \Delta\mathbf{q}_{smh}^{b} \tag{7f}$$

$$\Delta\mathbf{p}_{smh} = \eta_m \Delta\mathbf{q}_{smh}^{d} \tag{7g}$$

$$-\mathbf{X}_{3,5}^{\intercal} \cdot \mathbf{r}_{mh}^{\mathrm{hyd},\downarrow} \leq \Delta\mathbf{p}_{smh} \leq \mathbf{X}_{3,5}^{\intercal} \cdot \mathbf{r}_{mh}^{\mathrm{hyd},\uparrow} \tag{7h}$$

$$\mathrm{F}^0(\Delta\mathbf{q}_{smh}^{o}) = 0, \;\; h \neq N \tag{7i}$$

$$\mathrm{F}^0(\Delta\mathbf{q}_{smh}^{b}) = 0, \;\; h \neq N \tag{7j}$$

$$\mathbf{0} \leq \mathbf{X}_{4,6}^{\intercal} \cdot \mathbf{w}_{mh} + \Delta\mathbf{w}_{smh} \leq V_m\mathbf{1} \tag{7k}$$

$$\mathbf{0} \leq \mathbf{X}_{3,5}^{\intercal} \cdot \mathbf{q}_{mh}^{d} + \Delta\mathbf{q}_{smh}^{d} \leq Q_m^{d}\mathbf{1} \tag{7l}$$

$$\mathbf{0} \leq \mathbf{X}_{3,5}^{\intercal} \cdot \mathbf{q}_{mh}^{b} + \Delta\mathbf{q}_{smh}^{b} \leq Q_m^{b}\mathbf{1} \tag{7m}$$

$$\mathbf{0} \leq \mathbf{X}_{3,5}^{\intercal} \cdot \mathbf{q}_{mh}^{o} + \Delta\mathbf{q}_{smh}^{o} \tag{7n}$$

$$\mathbf{0} \leq \mathbf{X}_{3,5}^{\intercal} \cdot \mathbf{q}_{mh}^{\mathrm{rel}} + \Delta\mathbf{q}_{smh}^{\mathrm{rel}} \tag{7o}$$

$$\Delta\mathbf{q}_{smh}^{o} = \Delta\mathbf{q}_{smh}^{o+} - \Delta\mathbf{q}_{smh}^{o-} \tag{7p}$$

$$\Delta\mathbf{q}_{smh}^{b} = \Delta\mathbf{q}_{smh}^{b+} - \Delta\mathbf{q}_{smh}^{b-} \tag{7q}$$

$$\Delta\mathbf{p}_{smh} = \Delta\mathbf{p}_{smh}^{+} - \Delta\mathbf{p}_{smh}^{-} \tag{7r}$$

$$\mathbf{0} \leq \Delta\mathbf{q}_{smh}^{o\pm}, \Delta\mathbf{q}_{smh}^{b\pm}, \Delta\mathbf{p}_{smh}^{\pm}. \tag{7s}$$

The change in volume and flow between the reservoirs, (7a)–(7g), are analogous to the first-stage constraints (4a)–(4g). Note that the inflow is deterministic and is not part of the second-stage volume and flow deviation constraints. The change in hydropower production is constrained to be within the bounds of the procured reserve capacity in (7h), and the spillage and bypass is forced to remain C^0 continuous in the second stage by (7i) and (7j). The total volume, discharge and bypass in the second stage must still be within their respective physical bounds, which is ensured by constraining the sum of the first-stage and second-stage variables in (7k)–(7m). Similarly, the total spillage and reservoir release is kept non-negative by adding (7n) and (7o). The change in spillage,

bypass and hydropower production are split into positive and negative parts in (7p)–(7s). As was the case for the change in thermal generation, the split of the second-stage hydropower production variables is done to identify upward and downward reserve deployment correctly.

3) System constraints: The deviation between realized wind power and forecasted wind power, $\Delta\mathbf{W}_{sah}$, must be balanced in the second stage for all time intervals $h \in \mathcal{T}_{scen}$. In addition, the future expected cost of the system, z_s, is taken into account:

$$z_s \geq \sum_{m\in\mathcal{M}} WV_{mk}(v_{m,N+1} + \Delta v_{sm,N+1}) + D_k \tag{8a}$$

$$\sum_{m\in\mathcal{M}_a} \Delta\mathbf{p}_{smh} + \sum_{j\in\mathcal{J}_a} \Delta\mathbf{g}_{sjh} - \sum_{l\in\mathcal{L}} G_{la}\Delta\mathbf{f}_{slh} = -\Delta\mathbf{W}_{sah} - \mathbf{y}^{\text{shd}}_{sah} + \mathbf{y}^{\text{crt}}_{sah} \tag{8b}$$

$$-F_l^{max}\mathbf{1} \leq \mathbf{X}_{3,5}^{\intercal}\cdot\mathbf{f}_{lh} + \Delta\mathbf{f}_{slh} \leq F_l^{max}\mathbf{1} \tag{8c}$$

$$\mathrm{F}^0(\Delta\mathbf{f}_{slh}) = 0, \quad h \neq N \tag{8d}$$

$$\mathrm{F}^1(\Delta\mathbf{f}_{slh}) = 0, \quad h \neq N \tag{8e}$$

$$\sum_{m\in\mathcal{M}_a} \mathrm{F}^0(\Delta\mathbf{p}_{smh}) = 0, \quad h \neq N \tag{8f}$$

$$\sum_{m\in\mathcal{M}_a} \mathrm{F}^1(\Delta\mathbf{p}_{smh}) = 0, \quad h \neq N \tag{8g}$$

$$\mathbf{0} \leq \mathbf{y}^{\text{crt}}_{sah} \leq \max\{\mathbf{0}, \Delta\mathbf{W}_{sah}\} \tag{8h}$$

$$\mathbf{0} \leq \mathbf{y}^{\text{shd}}_{sah}. \tag{8i}$$

The expected cost of the hydrothermal system is bounded by the set of linear constraints $k \in \mathcal{K}$ in (8a), which depends on the total final volume of all hydropower reservoirs in scenario s. The coefficients WV_{mk} and constant term D_k are calculated by long-term hydrothermal scheduling models that consider the system operation on a time horizon of several seasons, such as [9]. The constraints are the result of the Benders decomposition scheme used in the long-term model, and the cuts can be used as end value description for the water in short-term models. Using more or less water in a given scenario results in higher or lower future expected costs according to these cut constraints. The power balance in (8b) allows the change in wind to be balanced by deploying thermal and hydropower reserves and changing the flow on the HVDC lines. In addition, wind curtailment and load shedding are possible options for keeping the balance. Note that (8h) only allow the curtailment of wind down to the forecasted wind power value. The total flow on HVDC lines are bound by the flow constraints in (8c), and is required to be C^1 continuous in (8d) and (8e). The C^1 continuity of the sum of the hydropower production is enforced directly by (8f) and (8g).

4) Initial continuity constraints: The continuity constraints applied to the second-stage variables in the previous subsections do not ensure a smooth transition from the schedule in the initial deterministic period to the real-time operation in each scenario. To remedy this, the following constraints based on (19)–(20) in Appendix A are added for all scenarios $s \in \mathcal{S}$:

$$\Delta\mathbf{g}^{(0)}_{sj,h_0}, \quad \Delta\mathbf{g}^{(1)}_{sj,h_0} = 0 \qquad \forall j \in \mathcal{J} \tag{9a}$$

$$\Delta\mathbf{f}^{(0)}_{sl,h_0}, \quad \Delta\mathbf{f}^{(1)}_{sl,h_0} = 0 \qquad \forall l \in \mathcal{L} \tag{9b}$$

$$\Delta\mathbf{q}^{b,(0)}_{sm,h_0} = 0 \qquad \forall m \in \mathcal{M} \tag{9c}$$

$$\Delta\mathbf{q}^{o,(0)}_{sm,h_0} = 0 \qquad \forall m \in \mathcal{M} \tag{9d}$$

$$\sum_{m\in\mathcal{M}} \Delta\mathbf{p}^{(0)}_{sm,h_0}, \quad \sum_{m\in\mathcal{M}} \Delta\mathbf{p}^{(1)}_{sm,h_0} = 0. \tag{9e}$$

Constraint (9a) force the thermal production and ramping in all scenarios to be continuous at time $t = h_0$ with respect to the scheduled first-stage production. The other constraints have a similar effect of enforcing C^0 and/or C^1 continuity at time $t = h_0$.

III. Case Study

In this section, the stochastic continuous-time model in Section II is used to investigate the behaviour of a hydro-thermal-wind system when additional wind power is integrated into the generation mix. A simplified Northern European system is used in the case study where Norwegian hydropower is coupled to Continental Europe with offshore wind power. This is a highly relevant use-case for the model, as Norwegian hydropower is seen as an important source of balancing in the European transition towards net zero emission.

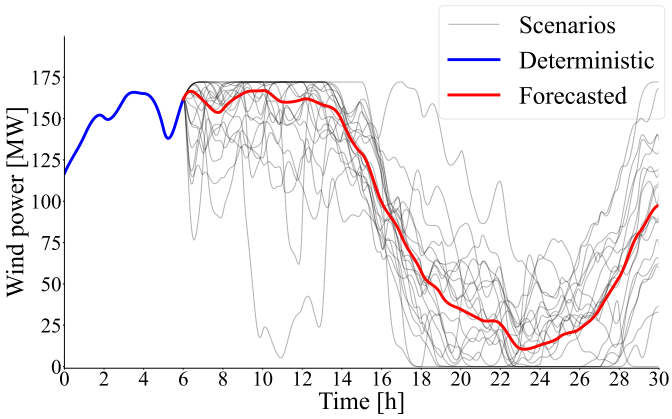

Fig. 2. Wind power input data used in the base case run of the stochastic continuous-time model. The wind power production in the first 6 hours is deterministic (blue line), while the forecasted wind power (red line) and wind power scenarios (black lines) apply for the following 24 hours.

A. System Description

The hydrothermal system used in the following sections is based on a simplified version of the Northern European system. An area containing only hydropower production is connected to a thermal area with an HVDC line, while a third wind power area is connected to the thermal area. This represents the coupling of the hydropower-dominated Norwegian system to the continental European system (Netherlands, Germany and Denmark) with considerable offshore wind power resources. A cascaded hydropower topology is used in the hydropower area, which is based on a real Norwegian watercourse with a total of 535.3 MW installed capacity divided among 12 linked reservoir-plant pairs, see [23] for a more detailed description of the hydropower system. The hydropower area is considered to represent the total Norwegian hydropower capacity of roughly 32 GW. The thermal units, HVDC cables, and installed wind power in the rest of the system are scaled down by an

This article has been accepted for publication in a future issue of this journal, but has not been fully edited. Content may change prior to final publication. Citation information: DOI 10.1109/TSTE.2022.3175430, IEEE Transactions on Sustainable Energy

equivalent amount to resemble a miniature Northern European system. The thermal area consists of 20 units (one nuclear, one oil, 9 gas, and 9 coal) picked from the 2019 update of the IEEE reliability test system [24]. After scaling the thermal units, a total of 921.2 MW thermal capacity is located in the thermal area. The transmission capacity between the hydropower and thermal areas amounts to 63 MW, while the offshore wind power capacity is 172 MW.

B. Input Data and Wind Power Scenario Generation

The linear cut constraints used in the future system value description in (8a) was calculated by the long-term hydropower scheduling model in [9] by optimizing the use of the hydrothermal system over a period of 156 weeks, and the initial volumes of every reservoir are set to 60% of its maximal volume. Inflow to the hydropower system are based on historic inflow data during winter, and is considered to be deterministic and is kept as a discrete hourly time series in the continuous-time model. The thermal marginal costs C_j were calculated based on the data in [24], and the same is true for the thermal startup and shutdown costs. The other cost parameters of the objective function are listed in Table I. The hydropower reserve capacity and activation costs are 40% and 30%, respectively, of an estimated "marginal cost" for the hydropower system based on the coefficients of the binding cut when the end volume is assumed to be the same as the initial volume. Similarly, the thermal reserve costs parameters are based on the marginal costs as suggested in [18].

TABLE I
OBJECTIVE FUNCTION COST PARAMETERS

Cost parameter	Symbol	Value
Bypass	C^b	100 €/Mm^3
Spillage	C^o	200 €/Mm^3
Bypass change	$C^{b\pm}$	$(1 \pm 0.1)C^b$
Spillage change	$C^{o\pm}$	$(1 \pm 0.1)C^o$
Hydropower startup, shutdown	$\overline{C}_m^{\text{hyd}}, \underline{C}_m^{\text{hyd}}$	100 €
Hydropower reserve capacity	K_m^{hyd}	9 €/MWh
Hydropower reserve activation	ρ^{hyd}	6.75 €/MWh
Thermal reserve capacity	K_j^{th}	$0.4C_j$
Thermal reserve activation	$C_j^{\pm}$	$(1 \pm 0.3)C_j$
Load shedding	C^{shd}	4500 €/MWh
Wind curtailment	C^{crt}	60 €/MWh

The generated wind power production scenarios, shown in Figure 2, are based on forecasted and realized wind power time series from western Denmark from October 2019 to April 2020 [25]. The stochastic model has a 6 hour period in the beginning which is deterministic, while the remaining 24 hours have uncertain wind power production. The piece-wise constant forecast error for each day was calculated in 15 min resolution, and this data was then fitted to a multivariate Gaussian kernel density function of 96 random variables. The tools in the SciPy package [26] in Python was used to fit the data to the multivariate Gaussian kernel. The estimated density function was then used to generate 200 equiprobable wind power deviation scenarios of 15 minute resolution and 24 hour length, which were added to the wind power forecast for October 14th, 2019 to create the full wind power scenarios. Values exceeding the wind power capacity or falling below zero were truncated to these limits. The scenarios were then reduced down to 20 by the standard backward scenario reduction algorithm [27]. The wind power data in the 6 hour long deterministic period is based on realized wind power from 18:00 to 24:00 on October 13th, and was inserted before the start of the 20 scenarios.

The discrete-time wind power scenarios were converted to continuous-time data suitable for the proposed optimization model by constructing a constrained least square error (LSE) optimization program. The quadratic LSE program finds the coefficients of Bernstein polynomials of degree 5 that best fit the piece-wise constant wind power data while taking into account continuity constraints and boundary conditions. The transition from the deterministic to the uncertain wind power period is especially important to consider in the LSE fit, as the values and derivatives of the wind power scenarios are all equal and continuous at the beginning of hour 7. The continuity constraints are imposed in the same way as in the full continuous-time optimization model presented in Section II, and the same is true for the upper and lower wind power limits.

The load for the hydropower area and thermal area are considered deterministic for the whole period, and is calculated based on load data from Norway and Germany from January 2nd 18:00 to January 3rd 24:00 in 2020 [28], [29]. The load series for the two areas are scaled down to have peaks of 85% of the installed thermal and hydropower capacity, respectively. The continuous-time load data was also created by fitting the piece-wise constant load data to Bernstein polynomials of degree 3 in a LSE optimization program.

C. Model Comparison and Results

The stochastic continuous-time hydrothermal model is implemented and solved using Pyomo [30], [31] and CPLEX 12.10 [32]. The extensive form of the stochastic model contains about 680k constraints and 420k variables, including 980 binary and 948 SOS 1 variables. A MIP gap of 0.09% (768 €) was reached after 72 hours on a machine with 24 CPUs at 3.50 GHz and 128 GiB RAM, though a reasonable gap of 0.78% was found after 16 hours. As noted in previous work such as [20], the calculation time of the continuous-time model is substantial for the relatively small system size of 20 thermal units and 12 hydropower plants. This can be attributed to several factors, such as the choice of polynomial degree in both model stages and the fact that no decomposition techniques have been employed. Solving the extensive form of any stochastic model quickly becomes intractable, and using Benders' decomposition or similar solution schemes would likely improve the calculation time. Such performance enhancement issues are not the focus of this paper, though it is an important factor in broadening the appeal of stochastic models in general.

Another model run identical to the first one except for a 50% increase in the system wind power energy was also solved. All wind power data was uniformly scaled by a factor of 1.5 for the second model run, and so the shape of the wind power

This article has been accepted for publication in a future issue of this journal, but has not been fully edited. Content may change prior to final publication. Citation information: DOI 10.1109/TSTE.2022.3175430, IEEE Transactions on Sustainable Energy

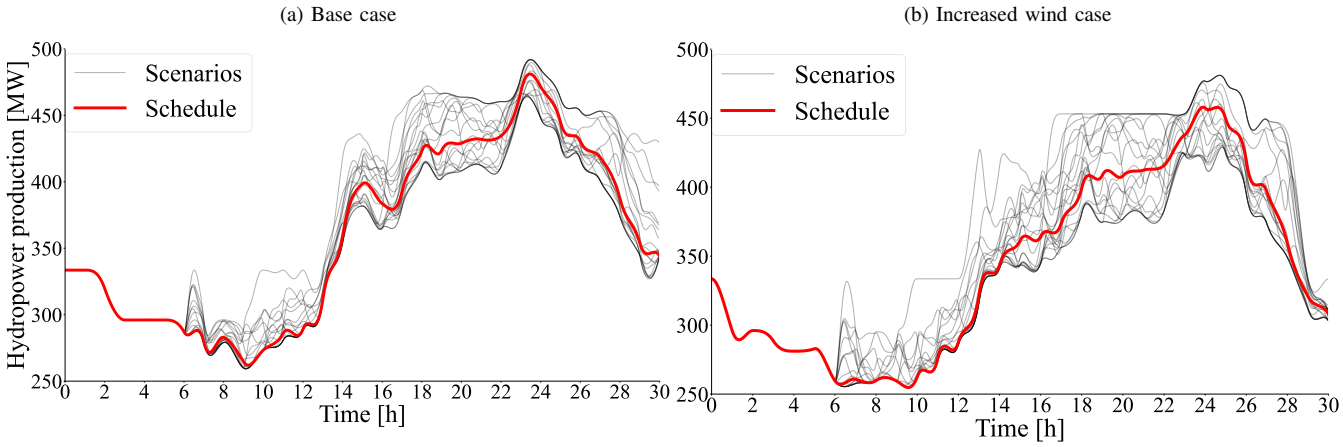

Fig. 3. The left and right figures show the hydropower production in the stochastic continuous-time model in the base case and the increased wind case, respectively. The red lines represent the planned production schedule (first-stage decisions) and the black lines show the realized hydropower production in the scenarios after reserve capacity has been activated (second-stage decisions).

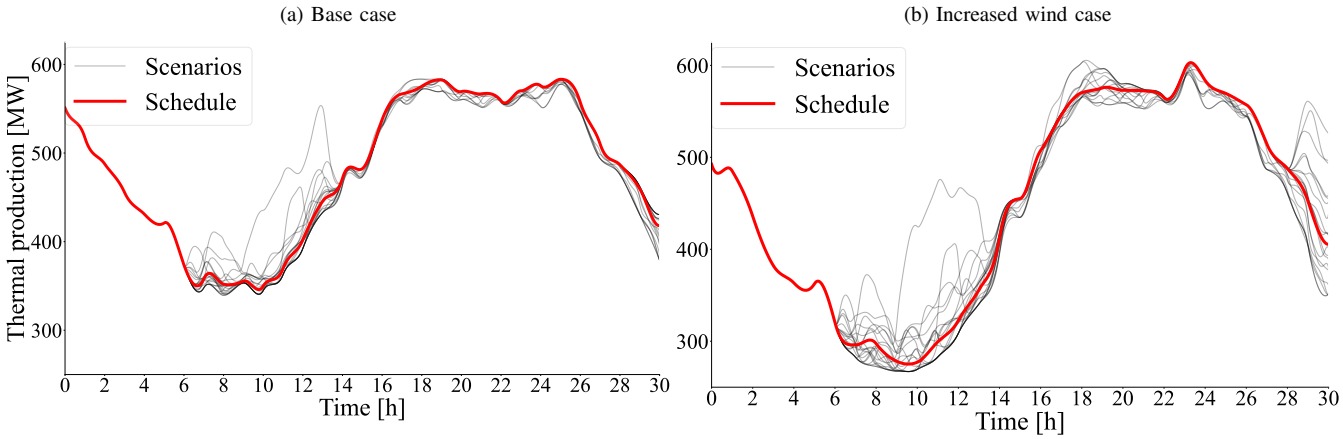

Fig. 4. The left and right figures show the thermal production in the stochastic continuous-time model in the base case and the increased wind case, respectively. The red lines represent the planned production schedule (first-stage decisions) and the black lines show the realized thermal production in the scenarios after reserve capacity has been activated (second-stage decisions).

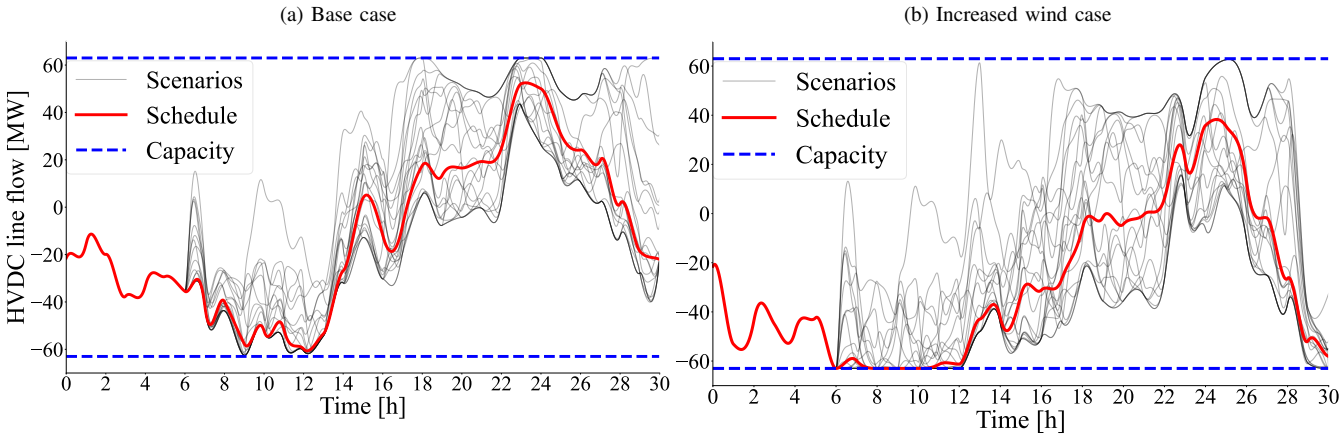

Fig. 5. The left and right figures show the flow of power on the HVDC line in the stochastic continuous-time model in for the base case and the increased wind case, respectively. The red lines represent the planned transmission schedule (first-stage decisions) and the black lines show the realized line flow in the scenarios (second-stage decisions). The blue dashed lines show the total transmission capacity of the HVDC cable. The flow is positive when moving from the hydropower area to the thermal area.

This article has been accepted for publication in a future issue of this journal, but has not been fully edited. Content may change prior to final publication. Citation information: DOI 10.1109/TSTE.2022.3175430, IEEE Transactions on Sustainable Energy

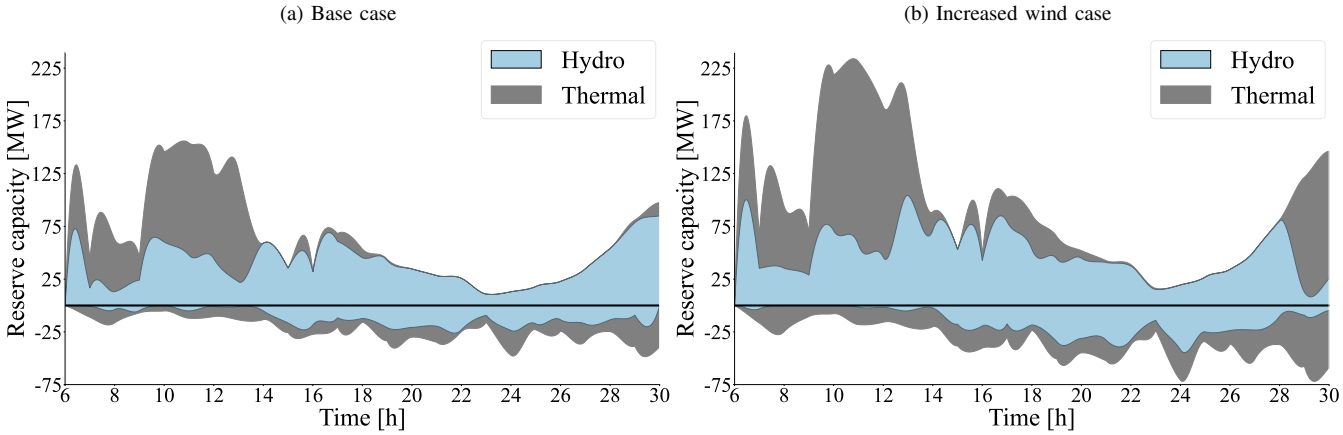

Fig. 6. A stacked plot of the total reserve capacity allocation on hydropower and thermal units in the base case and the increased wind case. The light blue region shows the total reserve capacity allocated on hydropower units, while the gray region is the total thermal reserve capacity allocation. Reserve capacity in the downward direction is shown as negative values.

TABLE II
AGGREGATED OPTIMIZATION RESULTS FOR THE TWO CASES. NEGATIVE LINE EXCHANGE SHOW A NET IMPORT TO THE HYDROPOWER AREA. RESERVE CAPACITY RESULTS ARE PRESENTED AS AVERAGE VALUES.

Sum quantity	Base case	Increased wind
Scheduled wind energy	3 041.6 MWh	4 562.3 MWh
Scheduled thermal energy	14 453.3 MWh	13 455.6 MWh
Scheduled hydro energy	10 805.7 MWh	10 282.7 MWh
Scheduled line exchange	-337.9 MWh	-860.9 MWh
Expected hydro bal. energy	293.1 MWh	373.2 MWh
Expected thermal bal. energy	105.6 MWh	224.6 MWh
Expected load shedding	0.1 MWh	0.7 MWh
Expected wind curtailment	21.8 MWh	33.4 MWh
Hydro reserve capacity up	39.8 MWh/h	50.0 MWh/h
Thermal reserve capacity up	24.7 MWh/h	45.9 MWh/h
Hydro reserve capacity down	12.0 MWh/h	16.0 MWh/h
Thermal reserve capacity down	11.4 MWh/h	18.9 MWh/h

scenarios and forecast is the same as in Figure 2. All other input data was kept the same for the two cases. The model with increased wind power reached a MIP gap of 0.83% in the 72 allotted hours, showing that it is more demanding to solve compared to the base case with less wind power. The purpose of the second case with more wind power is to investigate how the system will handle the variations of a substantial amount of new wind power capacity and how the flexible units are used in the real-time balancing to deal with the uncertainty of wind power. Aggregated numerical results for the two model runs are shown in Table II, and Figures 3 to 5 show the aggregated hydropower generation, thermal generation, and the line flow for both cases.

Table II is split into three sections, where the first one lists the total scheduled power generation for the different generation types, as well as the aggregated scheduled HVDC flow from the hydropower to the thermal area. Note that "scheduled" production and line flow means the first-stage solution of the production and flow variables over the 30 hour horizon. The 50% increase in wind power from the base case to the increased wind case equates to 1520.7 MWh additional forecasted wind energy. Since the load is equal in both cases, the extra wind energy displaces some of the thermal and hydropower production in the system. The total thermal generation is reduced by 997.7 MWh in the increased wind case, while the hydropower generation is reduced by 523.0 MWh. The strong temporal coupling imposed by the continuity constraints in the continuous-time model formulation restricts the model from abruptly changing thermal power output to accommodate the wind power. The wind power scenarios are also out of phase relative to the peak load in the system, which means that the system must deal with a steeper ramping in the net load in the increased wind power case. This can clearly be seen in the thermal generation results shown in Figure 4. The thermal power production in the increased wind case has a much lower minimum production and a higher peak production compared to the base case. This results in a steeper and longer ramping period in the thermal area, which is challenging for the ramping constrained thermal units. However, the solution is still feasible under the tight continuous-time thermal ramping constraints. The total energy exchange between the hydropower and thermal areas are negative in both cases, signifying that the hydropower area is a net importer of power. The net import is increased by over 150% in the increased wind case, which is equal to the decrease in hydropower production. In the increased wind case, Figure 5 shows that the scheduled flow from the thermal area to the hydropower area is at the line capacity in the peak wind power hours from 6 to 12, which means that the hydropower system is absorbing as much of the wind power as possible in this period. This limits the ability of using the hydropower for downward balancing energy, and the thermal units must be used for this purpose in the congested period.

The numbers in the second section of Table II shows the expected balancing energy delivered from hydropower and thermal units, in addition to the expected load shedding and wind curtailment. Note that the balancing energy is calculated as the sum of the absolute value difference between the first-stage scheduled production and the second-stage scenario production. Both the cases show that the hydropower resources are used for system balancing to a large extent, contributing 73.5% of the total balancing energy in the base case. The

hydropower covers virtually all of the system balancing in the upward ramping period from hour 14 to 18 in both cases, which allows the thermal units to ramp up to cover the peak load. The amount of balancing energy delivered from thermal units is drastically higher in the increased wind case compared to the base case, which shows the limit for how much the hydropower system can contribute to the overall system balancing. Part of this limitation is due to the congested HVDC line from hour 6 to 12 as discussed earlier. Another reason is the imposed smoothness and tight time-coupling of the hydrothermal continuous-time formulation, which implicitly captures the systems ability to react to fast sub-hourly variations in a more realistic way compared to analogous discrete-time models.

The average total reserve capacity procured on the hydropower and thermal units is shown in the final section of Table II, while Figure 6 shows the allocated reserve capacity as a function of time. Note that the unit in the table is denoted as MWh/h, indicating that it is the average reserve capacity delivered over the 24 hour stochastic period. The total procured reserve capacity increases by roughly 49% in both directions in the increased wind case, with the thermal units providing more downward reserve capacity than the hydropower units. The increased wind case requires a substantial amount of extra upward reserve capacity between hours 6 and 12 to balance the lack of wind in some of the scenarios compared to the base case, as shown in Figure 6. Note that the first six deterministic hours are not shown in the figure since zero reserve capacity is allocated in this period. The hydropower is able to provide all of the upward reserve capacity between hour 19 and 29 (peak net load period) in the base case due to the relatively low wind power output. The thermal units are required to take some of this burden in the increased wind case. Figure 3 shows that the hydropower production in most scenarios reach a flat upper plateau between hour 18 and 24 in the increased wind case, signifying that the online hydropower units are producing at maximum capacity.

IV. Conclusion

In this paper, a stochastic continuous-time hydrothermal model with uncertain wind power was presented. It models both structural imbalances and forecast deviations, and is well suited for investigations of the short-term balancing impacts of integrating large amounts of VRES into an existing hydrothermal system. The continuous-time model accurately estimates the flexibility of the combined system by enforcing smooth operation while accounting for activation of reserve capacity to balance wind power variations. The presented model serves as a theoretical benchmark for optimal coordination of flexible hydropower units, conventional thermal generation, and intermittent wind power generation. The proposed method can be applied to the other hybrid power system in order to characterize the variability and stochasticity of uncertain energy sources.

The case study in Section III uses a simplified Northern European system to show that hydropower can contribute significantly to the balancing of the interconnected system. The hydropower provided 73.5% of the balancing energy in the base case, which allows the thermal units time to ramp up to cover the peak net load in the thermal area. When the installed wind power capacity is increased by 50%, the hydropower is pushed towards its limits for providing balancing services. This is in part due to limited transmission capacity between the areas, which forces an increased use of thermal units for real-time balancing.

Finding ways of improving the calculation time of stochastic continuous-time models with energy storage is an important path of future research. Applying Lagrange relaxation schemes to complicating constraints could prove an effective way of decomposing continuous-time models. The continuity constraints are a prime candidate for such decomposition, since they couple the model both in time and across polynomial coefficients. It is very computationally demanding to solve the model presented in this paper, and efficient solution schemes are required before it can be solved for larger systems. Performing sensitivity analysis over multiple axis to show the robustness of the solution would also become practicable with lower solution times.

Acknowledgment

The authors would like to thank Dr. Bosong Li for helpful comments in the early stages of this work.

Appendix
Fundamental properties and notation

For further reading and references concerning the properties mentioned here, the reader is directed to [15] and Appendix C in [33]. In the continuous-time framework, time-dependent input data and variables are described by Bernstein polynomials of a finite degree n. There are $n+1$ of these polynomials:

$$B_{in}(t) = \binom{n}{i} t^i (1-t)^{n-i}, \quad i \in \{0, 1, ..., n\}, \tag{10}$$

and they form a basis for polynomials of positive degree less than or equal to n on the time interval $t \in [0, 1]$. Vector notation simplifies further definitions, denoted using bold text:

$$\mathbf{B}_n(t) = \left[B_{0n}(t), B_{1n}(t), ..., B_{nn}(t)\right]^\mathsf{T}. \tag{11}$$

A continuous curve $x(t)$ on the interval $t \in [0, 1]$ can be constructed by finding the vector of appropriate polynomial coefficients $\mathbf{x}$ such that:

$$x(t) = \mathbf{x}^\mathsf{T} \cdot \mathbf{B}_n(t). \tag{12}$$

The curve $x(t)$ is easily bounded by the use of the convex hull property, which guarantees that the curve is confined within the limits of the coefficients:

$$\mathbf{x} \leq x^{max}\mathbf{1} \quad \Rightarrow \quad x(t) \leq x^{max}. \tag{13}$$

Note that $\mathbf{1}$ denotes a constant vector of ones with appropriate length, which is used to describe the constant x^{max} in polynomial space since $\mathbf{1}^\mathsf{T} \cdot \mathbf{B}_n(t) = 1$. When using the representation in (12), the derivatives and integrals of $x(t)$ can be described by the linear relationships:

$$\frac{d\mathbf{B}_n(t)}{dt} = \mathbf{K}_n \cdot \mathbf{B}_{n-1}(t) \tag{14}$$

$$\int \mathbf{B}_n(t)dt = \mathbf{N}_n \cdot \mathbf{B}_{n+1}(t) \tag{15}$$

$$\int_0^1 \mathbf{B}_n(t)dt = \frac{1}{n+1}\mathbf{1}, \tag{16}$$

where $\mathbf{K}_n$ and $\mathbf{N}_n$ are matrices of size $(n+1)\times n$ and $(n+1)\times(n+2)$, respectively. As the Bernstein polynomials form a basis, Bernstein polynomials of degree n can be represented as Bernstein polynomials of any higher degree m by using the $(n+1)\times(m+1)$ elevation matrix $\mathbf{X}_{nm}$:

$$\mathbf{B}_n(t) = \mathbf{X}_{nm}\mathbf{B}_m(t), \quad n \leq m. \tag{17}$$

The definition in (12) can be extended to form a piece-wise polynomial representation of the curve $x(t)$ on a longer time horizon $t \in [0, N]$. The time horizon is first discretized into several time intervals $h \in \mathcal{T}$ of length δ_h, then the curve can be represented as:

$$x(t) = \mathbf{x}_h^\intercal \cdot \mathbf{B}_n\left(\frac{t-t_h}{\delta_h}\right), \qquad t_h \leq t \leq t_{h+1}. \tag{18}$$

Here, t_h represents the start time of interval h. To enforce continuity on $x(t)$ in the change from interval h to $h+1$, two functions F^0 and F^1 are defined as follows:

$$\mathrm{F}^0(\mathbf{x}_h) = \mathbf{x}_h^{(n)} - \mathbf{x}_{h+1}^{(0)} \tag{19}$$

$$\mathrm{F}^1(\mathbf{x}_h) = \mathbf{x}_h^{(n)} - \mathbf{x}_h^{(n-1)} - \mathbf{x}_{h+1}^{(1)} + \mathbf{x}_{h+1}^{(0)}, \tag{20}$$

where the notation $\mathbf{x}_h^{(j)}$ represents the jth vector component. The constraints $\mathrm{F}^0(\mathbf{x}_h) = 0$ and $\mathrm{F}^1(\mathbf{x}_h) = 0$ impose continuous values and derivatives on $x(t)$ over the interval change, respectively.

The time-dependent input data and decisions of the continuous-time model formulated in Section II are based on the definitions and properties in this appendix. The decision variables of the model become the vector coefficients of the Bernstein polynomials in addition to binary unit commitment variables, and a mixed integer linear problem formulation is recovered.

REFERENCES

[1] "Available online, accessed dec 2021," https://ec.europa.eu/clima/policies/strategies/2050.

[2] Q. P. Zheng, J. Wang, and A. L. Liu, "Stochastic optimization for unit commitment - A review," *IEEE Trans. Power Syst.*, vol. 30, no. 4, jul 2015.

[3] I. Pavic, M. Beus, H. Pandzic, T. Capuder, and I. Stritof, "Electricity markets overview - Market participation possibilities for renewable and distributed energy resources," in *14th Int. Conf. Eur. Energy Mark. (EEM)*, jul 2017.

[4] T. Weissbach and E. Welfonder, "High frequency deviations within the European power system: Origins and proposals for improvement," in *IEEE/PES Power Syst. Conf. Expo. (PSCE)*, 2009.

[5] M. Persson and P. Chen, "Frequency evaluation of the Nordic power system using PMU measurements," *IET Gener. Transm. Distrib.*, vol. 11, no. 11, aug 2017.

[6] C. Koch and L. Hirth, "Short-term electricity trading for system balancing: An empirical analysis of the role of intraday trading in balancing Germany's electricity system," *Renew. Sustain. Energy Rev.*, vol. 113, oct 2019.

[7] G. Fridgen, A. Michaelis, M. Rinck, M. Schöpf, and M. Weibelzahl, "The search for the perfect match: Aligning power-trading products to the energy transition," *Energy Policy*, vol. 144, sep 2020.

[8] IEA, "Offshore wind outlook 2019," IEA, Tech. Rep., 2019, https://www.iea.org/reports/offshore-wind-outlook-2019.

[9] A. Helseth, B. Mo, A. L. Henden, and G. Warland, "Detailed long-term hydro-thermal scheduling for expansion planning in the Nordic power system," *IET Gener. Transm. Distrib.*, vol. 12, no. 2, 2018.

[10] M. E. P. Maceira, D. D. Penna, A. L. Diniz, R. J. Pinto, A. C. Melo, C. V. Vasconcellos, and C. B. Cruz, "Twenty years of application of stochastic dual dynamic programming in official and agent studies in Brazil - main features and improvements on the NEWAVE model," in *20th Power Syst. Comput. Conf. (PSCC)*, aug 2018.

[11] A. L. Diniz, F. D. S. Costa, M. E. Maceira, T. N. Dos Santos, L. C. B. Dos Santos, and R. N. Cabral, "Short/Mid-term hydrothermal dispatch and spot pricing for large-scale systems - The case of Brazil," in *20th Power Syst. Comput. Conf. (PSCC)*, aug 2018.

[12] H. I. Skjelbred, J. Kong, and O. B. Fosso, "Dynamic incorporation of nonlinearity into MILP formulation for short-term hydro scheduling," *Int. J. Electr. Power Energy Syst.*, vol. 116, mar 2020.

[13] G. Morales-España, L. Ramírez-Elizondo, and B. F. Hobbs, "Hidden power system inflexibilities imposed by traditional unit commitment formulations," *Applied Energy*, vol. 191, apr 2017.

[14] M. Parvania and A. Scaglione, "Generation ramping valuation in day-ahead electricity markets," in *2016 49th Hawaii International Conference on System Sciences (HICSS)*, 2016, pp. 2335–2344.

[15] ——, "Unit commitment with continuous-time generation and ramping trajectory models," *IEEE Trans. Power Syst.*, vol. 31, no. 4, jul 2016.

[16] A. Zlotnik, L. Roald, S. Backhaus, M. Chertkov, and G. Andersson, "Coordinated scheduling for interdependent electric power and natural gas infrastructures," *IEEE Trans. Power Syst.*, vol. 32, no. 1, jan 2017.

[17] K. Hreinsson, A. Scaglione, and B. Analui, "Continuous time multi-stage stochastic unit commitment with storage," *IEEE Trans. Power Syst.*, 2019.

[18] R. Khatami and M. Parvania, "Stochastic multi-fidelity scheduling of flexibility reserve for energy storage," *IEEE Trans. Sustain. Energy*, 2019.

[19] R. Khatami, M. Parvania, and A. Narayan, "Flexibility reserve in power systems: Definition and stochastic multi-fidelity optimization," *IEEE Trans. Smart Grid*, vol. 11, no. 1, jan 2020.

[20] C. Ø. Naversen, A. Helseth, B. Li, M. Parvania, H. Farahmand, and J. P. S. Catalão, "Hydrothermal scheduling in the continuous-time framework," *Electr. Power Syst. Res.*, vol. 189, dec 2020.

[21] M. L. Øvstebø, C. Ø. Naversen, A. Helseth, and H. Farahmand, "Continuous-time scheduling of a hydrothermal system with integration of offshore wind power," in *17th Int. Conf. Eur. Energy Mark. (EEM)*, sept 2020.

[22] J. Kong, H. I. Skjelbred, and O. B. Fosso, "An overview on formulations and optimization methods for the unit-based short-term hydro scheduling problem," *Electr. Power Syst. Res.*, vol. 178, jan 2020.

[23] C. Ø. Naversen, H. Farahmand, and A. Helseth, "Accounting for reserve capacity activation when scheduling a hydropower dominated system," *Int. J. Electr. Power Energy Syst.*, vol. 119, jul 2020.

[24] C. Barrows, E. Preston, A. Staid, G. Stephen, J. P. Watson, A. Bloom, A. Ehlen, J. Ikaheimo, J. Jorgenson, D. Krishnamurthy, J. Lau, B. McBennett, and M. O'Connell, "The IEEE reliability test system: A proposed 2019 update," *IEEE Trans. Power Syst.*, vol. 35, no. 1, jan 2020.

[25] "Available online, accessed dec 2021," https://www.energidataservice.dk.

[26] P. Virtanen *et al.*, "SciPy 1.0: Fundamental algorithms for scientific computing in Python," *Nature Methods*, vol. 17, 2020.

[27] J. Dupačová, N. Gröwe-Kuska, and W. Römisch, "Scenario reduction in stochastic programming - An approach using probability metrics," *Math. Program. Ser. B*, vol. 95, no. 3, mar 2003.

[28] "Available online, accessed dec 2021," https://www.nordpoolgroup.com.

[29] "Available online, accessed dec 2021," https://transparency.entsoe.eu.

[30] M. L. Bynum, G. A. Hackebeil, W. E. Hart, C. D. Laird, B. L. Nicholson, J. D. Siirola, J.-P. Watson, and D. L. Woodruff, *Pyomo–optimization modeling in python*, 3rd ed. Springer Science & Business Media, 2021, vol. 67.

[31] W. E. Hart, J.-P. Watson, and D. L. Woodruff, "Pyomo: Modeling and solving mathematical programs in python," *Mathematical Programming Computation*, vol. 3, no. 3, 2011.

[32] IBM, "IBM CPLEX Optimizer," URL: https://www.ibm.com/analytics/cplex-optimizer, accessed dec 2021.

[33] C. Ø. Naversen, "Modelling approaches for hydro-dominated system balancing," PhD thesis, Norwegian University of Science and Technology, 2021. Available at: https://hdl.handle.net/11250/2735828.

Christian Øyn Naversen (M' 2022) completed his M.Sc. in Applied Physics and Mathematics at the Norwegian University of Science and Technology (NTNU) in 2015, and received a PhD from the Department of Electric Power Engineering at the same university in 2021. He has been employed at SINTEF Energy Research as a research scientist since 2015. Application of advanced optimization techniques to the field of short-term hydropower scheduling is his main area of expertise.

Masood Parvania (SM' 2019) is an Associate Professor and the Associate Chair for Research and Advancement at the Department of Electrical and Computer Engineering at the University of Utah. His research interests include the operation, economics, and resilience of power and energy systems, as well as modeling and operation of interdependent critical infrastructures. Dr. Parvania currently serves as an Associate Editor for the IEEE Transactions on Power Systems, the IEEE Transactions on Smart Grid, and the IEEE Transactions on Sustainable Energy. He is currently the Chair of the IEEE Power and Energy Society (PES) Utah Chapter, Chair of the IEEE PES Bulk Power System Operation Subcommittee, and Chair of the IEEE PES Reliability, Risk and Probability Application (RRPA) Subcommittee.

Arild Helseth (SM'2021) received his M.Sc. and Ph.D. degrees in electrical power engineering from the Norwegian University of Science and Technology (NTNU), in 2003 and 2008, respectively. Currently, he is a Senior Research Scientist at SINTEF Energy Research, where he has been employed since 2008. His experience is within mathematical modeling and optimization algorithms applied to electricity markets and power systems, particularly within the field of generation scheduling in hydro-dominated systems.

Hossein Farahmand (SM' 2020) is currently a Professor with the Department of Electric Power Engineering, NTNU, and is the head of the Electricity Markets and Energy System Planning (EMESP) Research Group. His research interests include power market analysis and hydropower scheduling, power system balancing, local flexibility markets and flexibility operation in smart systems. He has been involved in several EU projects including INVADE H2020, EU FP7 TWENTIES, EU FP7 eHighway2050, and IRPWIND. He is a member of the International Energy Agency (IEA) Wind Task 25, the IEEE PES Task Force on Water-Power Systems, and representing Norway as an expert in Flexibility Markets in International Smart Grid Action Network (ISGAN)-Annex 9: market design for power system flexibility.